

# One-step Synthesis of Spherical Polyaniline/Graphene Composites by Microemulsion for Supercapacitors

Pengfei Zhu, Tao Yu, Shaohong Kang, Shiyu Guan\*

School of Materials Science and Engineering, East China University of Science and Technology, Mei Long Road 130, Shanghai 200237, P.R. China

\*E-mail: [syguan@ecust.edu.cn](mailto:syguan@ecust.edu.cn)

Received: 16 July 2016 / Accepted: 2 September 2016 / Published: 10 October 2016

---

A simple approach to achieve microspherical polyaniline/graphene (PANI/rGO) composites by microemulsion has been developed, and the composites are further used as electrode materials for supercapacitors. Compared to other methods, microemulsion polymerization is a thermodynamically stable and easy-processing method, where the formed micelles act as “soft templates” to form the stable morphologies according to the type and concentration of surfactants. The one-step process is that water-dispersible GO is directly added into the SDS micelles during the microemulsion polymerization. The spherical SDS micelles just attach on the GO nanosheets with large lateral size, while the small GO nanosheets may embed into internal of the micelles. So, the as-prepared PANI/rGO composites have two probable ideal structures. Due to their unique architecture and the synergistic effect between PANI and graphene, the as-prepared PANI/rGO composites show the maximum electrochemical capacity of  $495.9 \text{ F g}^{-1}$  at  $0.5 \text{ A g}^{-1}$ , excellent rate capability and improved cycling stability.

---

**Keywords:** polyaniline microspheres; microemulsion; graphene; supercapacitors.

## 1. INTRODUCTION

Supercapacitors are rising alternative energy storage devices applied in some implements, such as mobile electronic, electric vehicles and so on. Compared to batteries, they are usually safer, possess higher power density, have short charge/discharge time and longer cycle life [1-4]. Based on the energy storage mechanisms, supercapacitors are usually divided into two types: one is the electrical double-layer capacitor (EDLC), where the capacitance arises from electrostatic attraction between the charges at the interface of the electrode and the ions of electrolyte but is usually too low, and the other is pseudocapacitor, which derives from fast, reversible redox reactions on the surface or in the interior of active materials and usually holds high capacitance [5-7]. To some extent, the electrochemical

performances of supercapacitors are decided by the electrode materials. Activated carbon [8], transition-metal oxide [9] and conducting polymers [10] are widely used. Among the various electrode materials, polyaniline (PANI) is considered as one of the most promising electrode materials due to its high theoretical capacitance, easy synthesis and low cost [11-13]. However, it exhibits the disadvantages of relatively low conductivity and mechanical degradation caused by expanding and contracting of the polymer chain skeleton during charge/discharge process, which leads to the capacity degradation of PANI [14]. To solve the problems, high conductive carbon materials such as porous carbon, active carbon, CNTs and other carbon nanomaterials have been incorporated into PANI [8, 15]. However, the selection of suitable carbon materials to hybrid with PANI is the key to obtain excellent electrochemical properties.

Graphene, a monolayer structure of  $sp^2$  hybridized carbon atoms [16], has attracted more and more attention due to its intriguing excellent electrical conductivity, great mechanical strength, large specific surface area and so on [17-19]. The integration of PANI and graphene has been verified to improve the capacitance and the cycling stability of PANI. Generally, PANI/graphene composites can be prepared by various methods, such as simple mixing, electropolymerization and chemical oxidation polymerization. Shi et al [20] have obtained the flexible graphene/PANI nanofiber composite film by mechanical mixing, whose specific capacitance is  $210 \text{ F g}^{-1}$  at  $0.3 \text{ A g}^{-1}$ . Wang et al [21] have fabricated the PANI/graphene nanocomposites via in situ anodic electropolymerization for flexible electrode, and the specific capacitance is  $233 \text{ F g}^{-1}$ . Wu et al [22] have prepared the chemically modified graphene/PANI nanofiber composites by in situ polymerization, and its specific capacitance is  $480 \text{ F g}^{-1}$  at  $0.1 \text{ A g}^{-1}$ . However, these methods have some disadvantages such as extra complicated preparation process or poor control of ideal structure. So, it is important for us to find a simple and convenient way to construct the ideal microstructure [23-24]. Microemulsion polymerization is a thermodynamically stable and easy-processing method, where the micelles in solution can form three different morphologies: rod-like, sphere and hexahedral, based on the type and concentration of surfactants. Interestingly, the spheres have the highest specific surface area among these, which are beneficial for electron transfer and electrolyte ions diffuse. Li et al [25] have prepared the polyaniline doped with different sulfonic acid using the emulsion polymerization method, and the maximum specific capacitance of PANI is  $410.6 \text{ F g}^{-1}$  at  $0.1 \text{ A g}^{-1}$ . Hassan et al [26] have firstly obtained the PANI microsphere by microemulsion polymerization, and then mixed with graphene oxide (GO) nanosheets by simply ultrasonic, finally reduced to graphene by HI, whose specific capacitance is  $448 \text{ F g}^{-1}$  at  $0.5 \text{ A g}^{-1}$ . Ahmad et al [27] also prepare the conductive polyaniline/graphene nanocomposites via in situ emulsion polymerization with improved electrical conductivity.

In our work, we synthesize the microspherical polyaniline/graphene (PANI/rGO) composites by one-step adding the GO into the surfactants directly during the microemulsion polymerization and then chemical reduction of GO. There will be two probable ideal structures (Fig.1): one is that the PANI microspheres attach to the surface of graphene nanosheets with large lateral size while the other is that small nano-size graphene nanosheets probably embed in the PANI microspheres during the microemulsion polymerization. The as-prepared PANI/rGO composites have spherical structures which possess numerous pore structures inside the microspheres. What's more, these hybrid structures can maximize the synergistic effect between PANI and graphene. In detail, the PANI/rGO microsphere

composites used as electrode materials for supercapacitors show the improved electrochemical capacity performance of  $495.9 \text{ F g}^{-1}$  at  $0.5 \text{ A g}^{-1}$ , excellent rate capability and improved cycling stability.

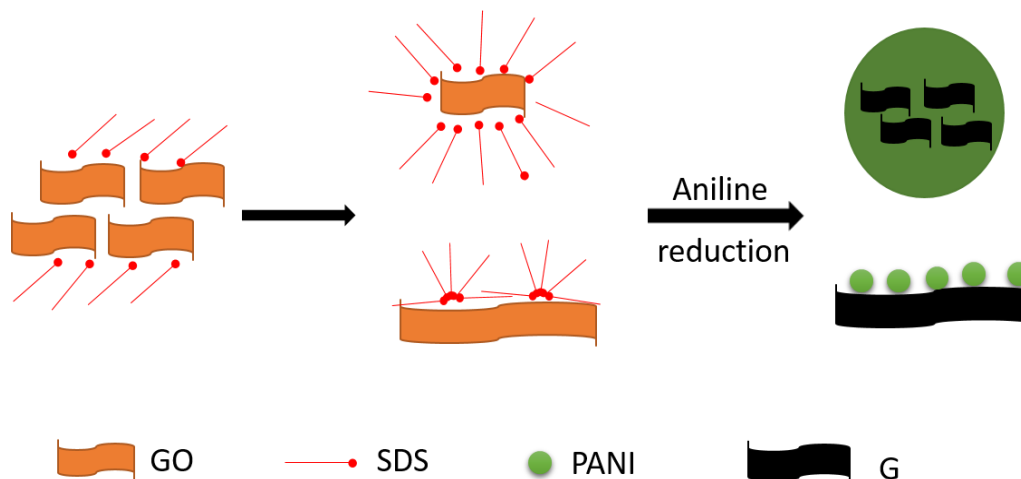


**Figure 1.** Illustration of the preparation of two types of PANI/G hybrids.

## 2. EXPERIMENTAL

### 2.1. Material

Aniline was purchased from Titan and distilled under vacuum and store at  $0 \text{ }^{\circ}\text{C}$ . The other reagents like ammonium peroxydisulfate (APS), sodium dodecyl sulfate (SDS), nature nano-graphite powder, ethanol,  $\text{H}_2\text{SO}_4$ , acetone were used without further purification.

### 2.2. Preparation of Graphene Oxide (GO)

Graphene oxide was prepared by the following modified Hummers method [28]: firstly, the mixture of graphite (2 g),  $\text{NaNO}_3$  (1.5 g) and 68 mL of concentrated  $\text{H}_2\text{SO}_4$  was cooled to  $0 \text{ }^{\circ}\text{C}$  in an ice bath and stirred for 5 min. After that  $\text{KMnO}_4$  (10 g) was added slowly and stirred for another 30 min continuously at low temperature ( $< 5 \text{ }^{\circ}\text{C}$ ). Then 100 mL distilled water was added slowly to this reaction mixture at room temperature and further heated to  $60 \text{ }^{\circ}\text{C}$ , keeping stirring for one and half hour continuously, and the color turned to mud brown. At the end, the mixture was further treated with 8 mL of 30%  $\text{H}_2\text{O}_2$  for one hour. The color turned into pale yellow from dark brown. For purification, the mixture was washed by centrifugation with diluted HCl and then deionized water for several times until the pH of the solution was near neutral. Finally, GO was dried under vacuum at  $50 \text{ }^{\circ}\text{C}$  for 24 h.

### 2.3. Preparation of PANI/rGO composites

PANI/rGO composites were synthesized through microemulsion polymerization [26] of aniline monomer with the existence of graphene oxide. The details of the procedure are described as

following: First, 30 mg GO was mixed with 30 mL deionized water, sonicated using an ultrasonicator (40 kHz) in water for 30 min. SDS (1.5 g) was added to the suspension and stirred continuously, while being heated to 60 °C. Then aniline (0.5 g) was dispersed in 5 mL of 1 M HCl (32 wt%) for 15 min, then mixed with 10 mL deionized water and subsequently dropped into the above microemulsion rapidly until the heater temperature reaching 60 °C. At the end, APS (62.5 mg) was mixed with 5 mL water and added into the reactor drop by drop. The reactor was kept stirring for 6 h. Then, the PANI/GO suspension was treated with ethanol to break the balance, and washed with deionized water until no bubble in the solution. In order to reduce the GO, hydrazine hydrate (80 wt%) were added and kept the mixture stirring and heating to 100 °C for 12 h, then the suspension was washed with deionized water, and re-doped with 100 mL 1 M HCl, subsequently filtered by a 0.2 µm PTFE membrane filter, vacuum dried, weighed and saved. The mixture was named as PANI/rGO-2. In addition, 15 mg, 60 mg and 120 mg GO were added to prepare various PANI/rGO composites, denoted as PANI/rGO-1, 3 and 4, respectively.

#### 2.4. Characterization

The Raman was measured by InVia Raman microscope (Renishaw, UK) with 514.5 nm diode laser excitation. FT-IR spectrum was recorded on a Nicolet 5700 spectrometer (Thermo Electron, America). FE-SEM was obtained on a S-3400 (Hitachi, Japan). TEM measurement was conducted on a JEM-1400 (JEOL, Japan) with embedded sections after slitting (LECIA EM UC7). AFM image was collected by a Veeco IIIa Multimode microscope, operated in tapping mode.

#### 2.5. Electrochemical tests

Electrochemical tests were conducted on a CHI660D electrochemical workstation in a three-electrode system. The working electrode consisted of active materials (80 wt%), acetylene black (10 wt%), and polyvinylidene fluoride (10 wt%) dispersed in NMP, and then coated the slurry onto the surface of carbon paper and dried. Additionally, Pt was used as the counter with the Ag/AgCl as reference electrode. galvanostatic charge/discharge and cyclic voltammetry (CV) tests were performed in a voltage range between 0~0.8 V and -0.2~0.8 V respectively, the specific capacitances could be calculated according to the formula:  $C_m = I \times t / (m \times U)$ , where  $I$  is the constant discharge current (A),  $t$  is the discharge time (s) obtained from the galvanostatic charge/discharge test. The electrochemical impedance spectroscopy (EIS) test was operated in the frequency range from 100 kHz to 0.01 Hz, and the cycling performance was performed at 2 A g<sup>-1</sup>.

### 3. RESULTS AND DISCUSSION

#### 3.1 Morphology and Structure

The dispersion behavior of exfoliated graphite oxide in aqueous solution under ultrasonic vibration is investigated by AFM. Fig. 2 shows the thickness of GO nanosheets is about ~ 2.0 nm and

the lateral size is ~ 240 nm. SEM observations were used to verify the morphology and structure of PANI/rGO-2 composites, providing a direct proof for the growth mechanism of PANI in the existence of rGO nanosheets and surfactant (SDS).

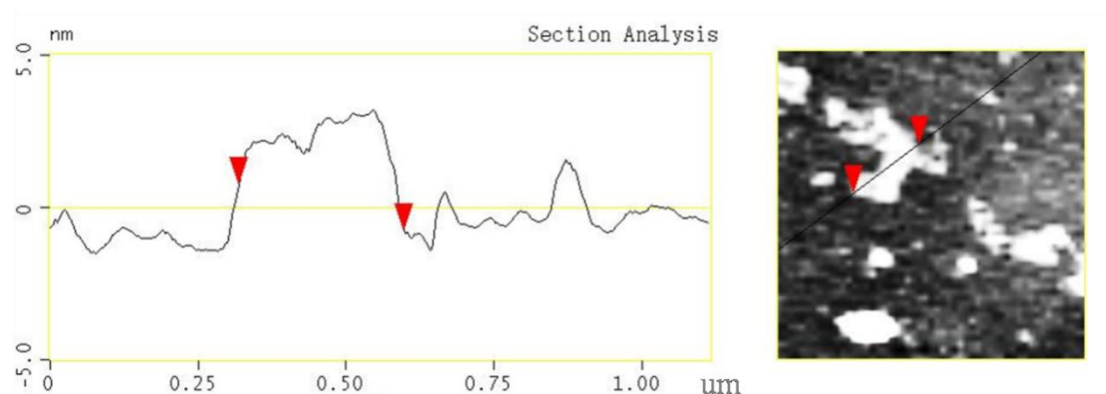


**Figure 2.** AFM image of exfoliated GO sheets

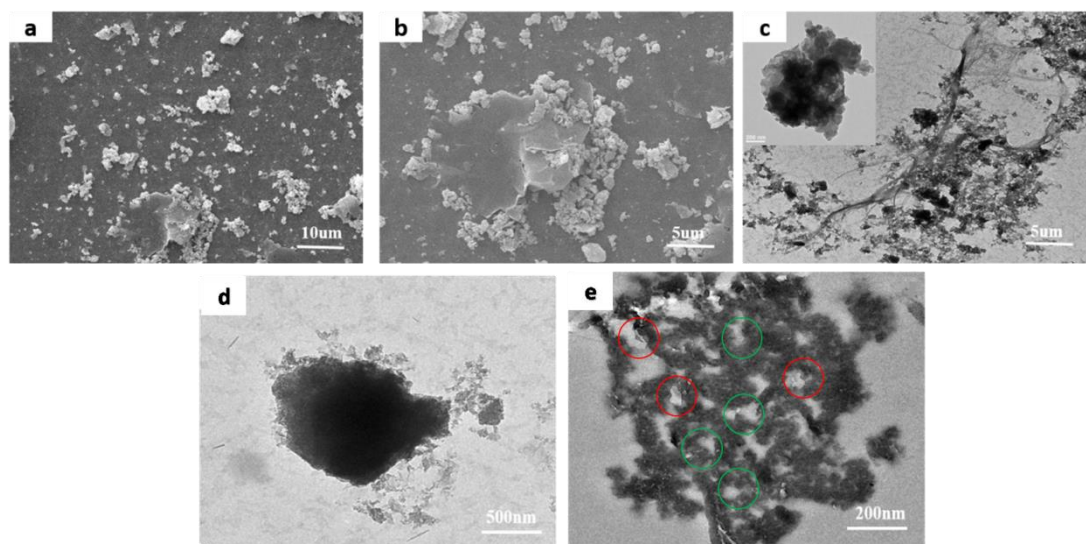


**Figure 3.** (I) SEM image of PANI/rGO-2 (a) and (b), TEM image of PANI/rGO-2 (c); (II) TEM image of microspherical PANI/rGO-2 (d), TEM image of embedded sections of microspherical PANI/rGO-2 after slitting (e).

The morphologies are divided into two types (I, II), as illustrated in Fig.1. On one hand, in Fig. 3a, granulated PANI shows quite rough surfaces with the diameter of 1-2  $\mu\text{m}$  and the rGO nanosheets are irregularly aggregated with the size of ~10  $\mu\text{m}$ . The enlarged image of PANI/rGO-2 composites (Fig. 3b) shows that a portion of PANI microspheres attach on the graphene flake or accumulate at the edge of rGO. TEM images of the hybrids (Fig.3c) well support SEM result. On the other hand, in Fig.3d, it is supposed that GO nanosheets are probably embedded into the internal of PANI microspheres according to the phenomenon that the few wrinkled GO nanosheets attach to the edge of PANI. To

further confirm the supposition, we slit the microsphere, and observe the section of PANI through resin entrapping and cutting. Fig. 3e reveals that the morphology of polyaniline microsphere with porous channels (green arrow), which are beneficial to the electrolyte infiltration and the ion transmission. In addition, the transparent and wrinkled flakes with the size of  $\sim 200$  nm can be obviously seen on the section after slitting in Fig. 3e (red arrow), which is probably attributed to the small lateral size GO nanosheets which disperse in the surfactant micelles. Upon adding an initiator, they are probably embedded into the matrix without destroying the sphere microstructure during the microemulsion polymerization.

The formation of different morphologies can be explained by the following: Before polymerization, graphene oxide nanosheets were dispersed by SDS used as emulsifier. A large amount of SDS can cover on the surface of graphene oxide. The aggregated and large-size GO nanosheets may act as an active site, and the well-dispersed small nano-size GO probably embedded into the micelles. When aniline monomer and APS initiator were added to the GO-surfactant dispersion in water, the components probably diffused into two sites due to their hydrophobic nature: (1) between the GO surfaces and surfactants, or (2) inside the surfactant micelles. During the microemulsion polymerization, on one hand, the hydrophobe aniline monomer diffused from the droplets into the GO layer. After that, the PANI microsphere was formed and attached on the surfaces of GO. On the other hand, small nano-size GO with stronger hydrophobic probably diffused into the micelles, and embedded into the microsphere PANI during the microemulsion polymerization.

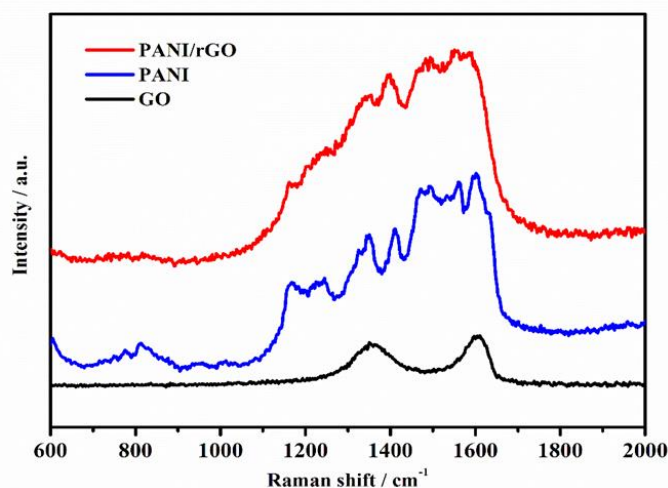


**Figure 4.** Raman spectra of GO, PANI and PANI/rGO

To validate successful hybrid, GO, PANI and PANI/rGO ( $m_{GO}=30$  mg) were characterized by Raman spectroscopy and FTIR. In Fig. 4, the Raman spectrum of the PANI has characteristic peaks around 800, 1160, 1325, 1466, and 1589  $\text{cm}^{-1}$ , which can be attributed to ring deformation of the benzene/quinoid rings, C-H bending of the benzene ring, protonated C-N stretching, C=N stretching,

and C-C stretching of the benzene/quinoid ring, respectively [29-31]. The as-prepared GO shows two main peaks at 1330 and 1590  $\text{cm}^{-1}$ , which correspond to G band of  $\text{sp}^2$  carbons and the D band of the disordered structure [32-33]. The spectrum of composite shows similar bands of emeraldine salt. Obviously, peaks around 800 and 1466  $\text{cm}^{-1}$  in the composite disappear due to the PANI superimposed on the graphene structures through the strong interaction between the PANI polymer backbone and the graphene nanosheets via  $\pi$ - $\pi$ stacking [34, 35].

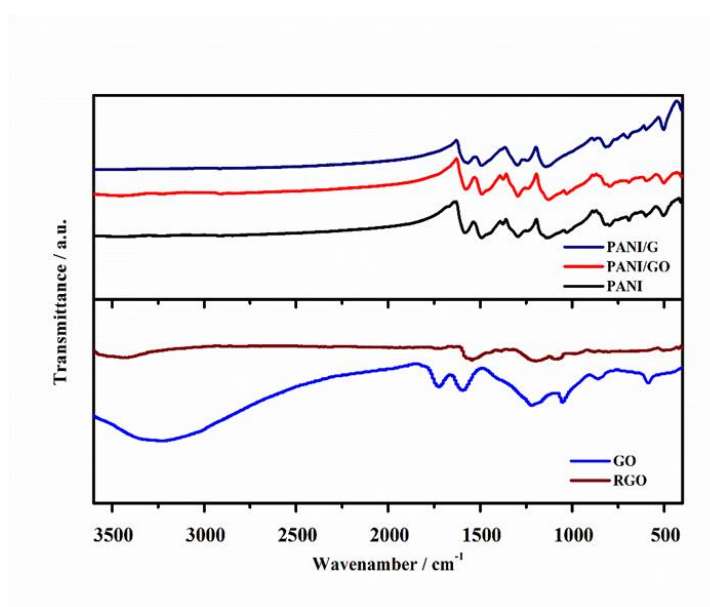


**Figure 5.** FT-IR spectra of GO, G, PANI and PANI/rGO

In Fig. 5, the FT-IR spectrum of the GO shows a broad peak at 3350  $\text{cm}^{-1}$  due to the O-H stretching vibration, and the peaks at 1730, 1400, 1225, and 1080  $\text{cm}^{-1}$  can be assigned to C-O stretching, C-OH groups, C-O (epoxy groups) stretching and the C-O (alkoxy groups) stretching [36]. However, the disappearance of characteristic peaks indicates the oxygen-containing groups of GO are reduced. The PANI has characteristic peaks at 1565 and 1478  $\text{cm}^{-1}$ , assigned to C=C stretching of the quinoid ring and benzenoid ring, respectively, and the peak at 1297  $\text{cm}^{-1}$  is due to the C-N stretching in a aromatic amine, the peak at 1110  $\text{cm}^{-1}$  corresponds to the C-N stretching in quinoid ring. The bending of aromatic C-H in the substituted benzene ring appeared in the 797  $\text{cm}^{-1}$  peak [37]. In PANI/GO and PANI/rGO composites, the characteristic peaks of PANI can be observed clearly, further verifying the formation of PANI in these two composites.

### 3.2. Electrochemical performance

To assess the electrochemical performances of pure PANI and PANI/rGO composites, electrochemical tests were performed in the condition of 1M  $\text{H}_2\text{SO}_4$  aqueous solution at room temperature. Figure. 6a shows the CV curves of PANI/rGO composite at different rates from 2 to 100  $\text{mV s}^{-1}$  in a voltage range between - 0.2 and 0.8 V vs Ag/AgCl. The PANI/rGO composite behaves the

symmetric aquasi-rectangular curves with small redox peaks at low scan rates, indicating their double-layer capacitor behavior. With the scan rate increases, the rectangular shape of CV curves disappears, but two pairs of redox peaks occur obviously, which are corresponded to the pseudocapacitive behavior of the redox reactions, especially at high scan rates. Fig. 6b shows the CV curves of pure PANI and PANI/rGO composite at a scan rate of  $5\text{ mV s}^{-1}$ . The CV area is proportional to the capacity and the area of PANI/rGO composites is larger than the pure PANI, which demonstrates that the specific capacitance of PANI/rGO-2 composite is higher than the pure PANI microspheres.

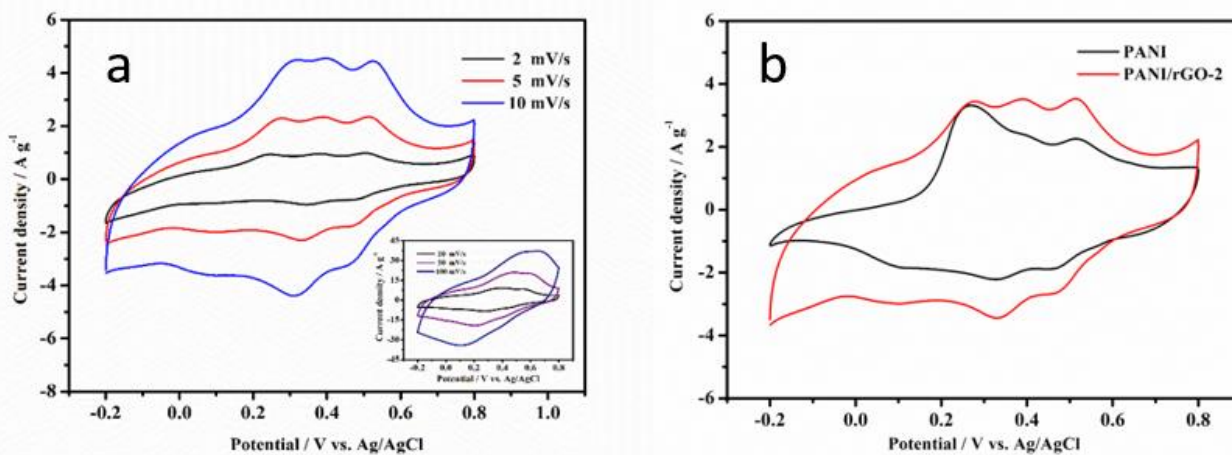
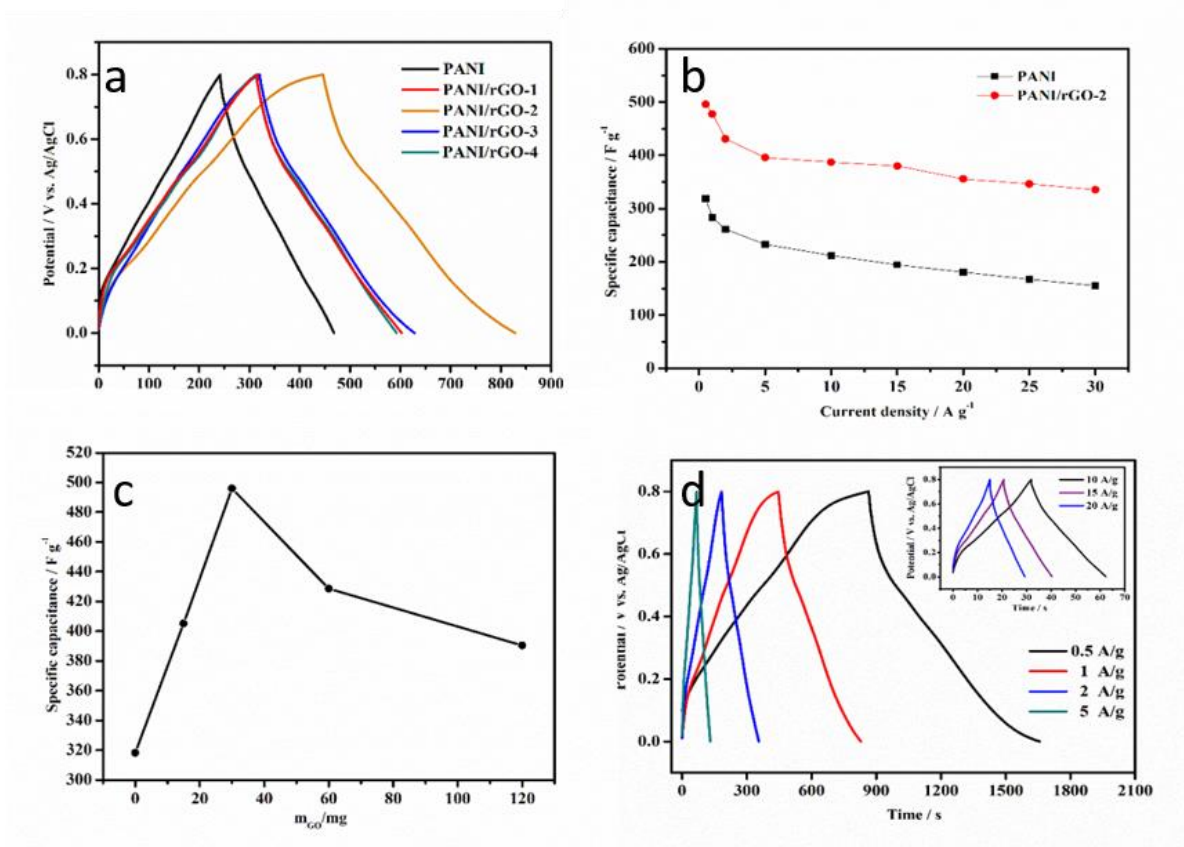


**Figure 6.** CV curves of PANI/rGO-2 at different scan rates (a); CV curves of PANI and PANI/rGO-2 at a constant scan rate of  $5\text{ mV s}^{-1}$  (b).

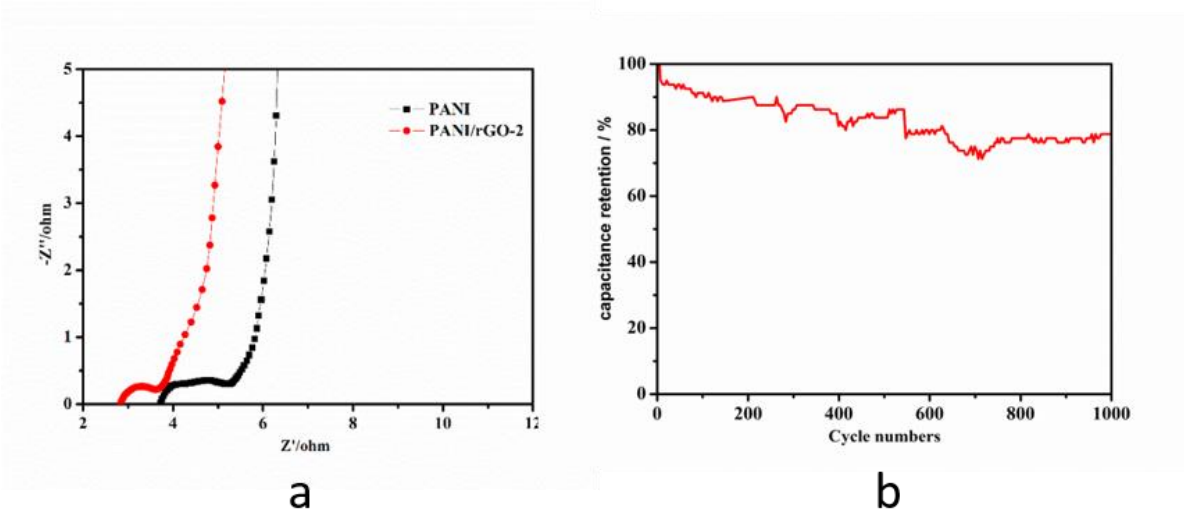
Fig. 7a shows the galvanostatic charge/discharge curves of pure PANI and PANI/rGO composites with different addition of GO during the emulsion polymerization at  $1\text{ A g}^{-1}$ . The discharge time of PANI/rGO is much longer than the pure PANI. Based on the calculation formula for specific capacitance, the specific capacitance is proportional to the discharge time in the galvanostatic charge/discharge curve, which suggests the specific capacitance of PANI/rGO composites is higher than the PANI. As showed in Fig. 7b and 7c, the PANI/rGO-2 composite displays the maximum specific capacitance of  $495.9\text{ F g}^{-1}$  at  $0.5\text{ A g}^{-1}$ , which is larger than the pure PANI ( $318.3\text{ F g}^{-1}$ ) and other composites, similar results have been demonstrated using the emulsion polymerization method in previous reports [25-27]. Further, a specific capacitance of  $355.5\text{ F g}^{-1}$  still remains when the current density increased to  $20\text{ A g}^{-1}$ , proving the good rate performance.

Fig. 8a shows the Nyquist plots of pure PANI and PANI/rGO-2 electrodes. Firstly, the equivalent series resistance (ZRe) value was estimated from the x-axis intercept, which is a combined resistance including ionic resistance of electrolyte, intrinsic resistance of substance and interface resistance. The value of ZRe is  $2.9\ \Omega$  for PANI/rGO-2 and  $3.8\ \Omega$  for pure PANI indicating that the conductivity for the composite is greater than the PANI. Secondly, the diameter of semicircle for composite in high frequency region is much smaller than the pure PANI indicating its lower contact and charge transfer resistance (Rct). Finally, at low frequency, the line of the PANI/rGO-2 composite is near parallel demonstrating the good capacitive behavior. Figure 8b shows the cyclic performance of

the PANI/rGO-2 composite examined by galvanostatic charge/discharge tests at  $2 \text{ A g}^{-1}$ . It still keeps the capacitance retention of the electrode 78.8% after 1000 times of charge-discharge cycling.



**Figure 7.** galvanostatic charge/discharge curves of PANI and PANI/rGO composites with different addition of GO during the emulsion polymerization at  $1 \text{ A g}^{-1}$  (a); the specific capacitance of PANI and PANI/rGO-2 at  $0.5 \sim 30 \text{ A g}^{-1}$  (b); the specific capacitance of PANI and PANI/rGO composites at  $1 \text{ A g}^{-1}$  (c); galvanostatic charge/discharge curves of PANI/rGO-2 at different current density (d).



**Figure 8.** Nyquist plots for PANI, PANI/rGO-2 (a); Cycling performance of PANI/rGO-2 at  $2 \text{ A g}^{-1}$  (b).

#### 4. CONCLUSIONS

In summary, we have developed a simple approach to achieve the microspherical PANI/rGO composites by microemulsion polymerization. According to the different dispersion types of SDS, the hybrids have two probable ideal microsphere structures. One is small nano-size GO nanosheets embedded into the microspherical PANI, and the other is PANI microsphere attached on the agglomerated GO nanosheets. Due to the microspherical structure of hybrid and the synergistic effect between PANI and graphene, the as-prepared PANI/rGO composites show good electrochemical performances, such as high specific capacitance ( $495.9 \text{ F g}^{-1}$  at  $0.5 \text{ A g}^{-1}$ ), excellent rate capability ( $355.5 \text{ F g}^{-1}$  retained at  $20 \text{ A g}^{-1}$ ) and improved cycling stability (78.8% of capacitance retention after 1000 charge/discharge cycles), and the PANI/rGO composites will be a promising electrode materials for supercapacitors.

#### ACKNOWLEDGEMENTS

The author are grateful for the financial support from National Natural Science Foundation of China (No.21274043)

#### References

1. P.M. Simon, Y. Gogotsi, *Nat. Mater.*, 7 (2008) 845.
2. B.E. Conway, *J. Electrochem. Soc.*, 138 (1991) 1539.
3. A.G. Pandolfo, A.F. Hollenkamp, *J. Power Sources*, 157 (2006) 11.
4. R. Kotz, M. Carlen, *Electrochim. Acta*, 45 (2000) 2483.
5. W. Xing, S.Z. Qiao, R.G. Ding, F. Li, G.Q. Lu, Z.F. Yan and H.M. Cheng, *Carbon*, 44 (2006) 216.
6. O. Barbieri, M. Hahn, A. Herzog and R. Kotz, *Carbon*, 43 (2005) 1303.
7. Z. Li, H. Zhang, Q. Liu, Y. Liu, L.A. Stanciu, and J. Xie, *Carbon*, (2014) 257.
8. Y.G. Wang, H.Q. Li, and Y.Y. Xia, *Advanced Materials*, 18 (2006) 2619.
9. Y.G. Wang, H.Q. Li, K. Purushothaman and G. Muralidharan, *ACS Appl. Mater. Interfaces*, 4 (2012) 4188.
10. G.A. Snook, P. Kao and A.S. Best, *J. Power Sources*, 196 (2011) 1.
11. H Li, J Wang, Q Chu, Z Wang, F Zhang and S Wang, *J. Power Sources*, 190 (2009) 578.
12. K.S. Ryu, K.M. Kim, N. Park, Y.J. Park and S.H. Chang, *J. Power Sources*, 103 (2002) 305.
13. V. Gupta and N. Miura, *Mater Lett.*, 60 (2006) 1466.
14. W. Chen and T. Wen, *J. Power Sources*, 117 (2003) 273.
15. D.D. Potphode, P. Sivaraman, S.P. Mishra and M. Patri, *Electrochim. Acta*, 155 (2015) 402.
16. M.J. Allen, V.C Tung and R.B. Kaner, *Chem. Rev.*, 110 (2010) 132.
17. A.H. Neto, F. Guinea, N.M. Peres, K.S. Novoselov and A.K. Geim, *Rev. Mod. Phys.*, 81 (2009) 109.
18. S. Stankovich, D.A. Dikin, G.H Dommett, K.M. Kohlhaas, E.J. Zimney, E.A. Stach, and R.S. Ruoff, *Nature*, 442 (2006).
19. M.D. Stoller, S. Park, Y. Zhu, J. An and R.S. Ruoff, *Nano Lett.*, 8 (2008).
20. Q. Wu, Y.X. Xu, Z.Y. Yao, A.R. Liu, and G.Q. Shi, *ACS Nano*, 4 (2010) 1963.
21. D.W. Wang, F. Li, J.Q. Zhao, W.C. Ren, Z.G. Chen, J. Tan, Z.S. Wu, I. Gentle, G.Q. Lu and H.M. Cheng, *ACS Nano*, 3 (2009) 1745.
22. K. Zhang, L.L. Zhang, X.S. Zhao and J.S. Wu, *Chem. Mater.*, 22 (2010) 1392.
23. H. Liu, W. Zhang, H. Song, X. Chen, J. Zhou and Z. Ma, *Electrochim. Acta*, 146 (2014) 511.
24. J. Luo, Q. Ma, H. Gu, Y. Zheng and X. Liu, *Electrochim. Acta*, 173 (2015) 184.

25. Y.C. Lin, X.X. Zhong, H.X. Huang, and H.Q. Wang, *Acta Physico-Chimica Sinica*, 32 (2016) 474
26. M. Hassan, K.R. Reddy, E. Haque, S.N. Faisal, S. Ghasemi, A.I. Minett and V.G. Gomes, *Compos Sci Technol.*, 98 (2014) 1.
27. B. Hossein , R.S.A. Ahmad , M. Shohreh, G. Fariba, *Synthetic Met.*, 196 (2014) 199.
28. W.S. Hummers, R.E. Offeman, *J. Am. Chem. Soc.*, 80 (1958) 1339.
29. N. Kumar, H. Choi, Y.R. Shin, D.W. Chang, L. Dai and J. Baek, *ACS Nano*, 6 (2012) 1715.
30. N.I. Kovtyukhova, P.J. Ollivier, B.R. Martin, T.E. Mallouk, S.A Chizhik, E. Buzaneva and A. Gorchinskiy, *Chem. Mater.*, 11 (1999) 771.
31. A. Ferrari, J.C. Meyer, V. Scardaci, C. Casiraghi, M. Lazzeri, F. Mauri and A.K. Geim, *Phys. Rev. Lett.*, 97 (2006) 187401.
32. J. Luo, S. Jiang, R. Liu, Y. Zhang and X. Liu. *Electrochim. Acta*, 96 (2013) 103.
33. W. Chidawanyika and T. Nyokong, *Carbon*, 48 (2010) 2831.
34. G. Zeb, P.E. Gaskell, X.T. Le, X. Xiao, T. Szkopek and M. Cerruti. *Langmuir*, 28 (2012) 13042.
35. J.M. Englert, C. Dotzer, G. Yang, M. Schmid, C. Papp, J.M. Gottfried and A. Hirsch, *Nat. Chem.*, 3 (2011) 279.
36. H. Guo, X. Wang, Q. Qian, F. Wang and X. Xia, *ACS Nano*, 3 (2009) 2653.
37. N. Xiao, H. Tan, J. Zhu, L. Tan, X. Rui, X. Dong and Q. Yan, *ACS Appl. Mater. Interfaces*, 5 (2013) 9656.

© 2016 The Authors. Published by ESG ([www.electrochemsci.org](http://www.electrochemsci.org)). This article is an open access article distributed under the terms and conditions of the Creative Commons Attribution license (<http://creativecommons.org/licenses/by/4.0/>).